Remote Sensing Applications: Society and Environment 35 (2024) 101224

Contents lists available at ScienceDirect

Remote Sensing Applications: Society and Environment

journal homepage: www.elsevier.com/locate/rsase

Biophysical characterization of summer Arctic sea-ice habitats using a remotely operated vehicle-mounted underwater hyperspectral imager

Benjamin A. Lange [a, b, *], Ilkka Matero [c, d], Evgenii Salganik [a, e], Karley Campbell [f], Christian Katlein [c], Philipp Anhaus [c], Janina Osanen [f], Mats A. Granskog [a]

[a] Norwegian Polar Institute, Fram Centre, Tromsø, Norway
[b] Norwegian Geotechnical Institute, Oslo, Norway
[c] Alfred Wegener Institute Helmholtz Centre for Polar and Marine Research, Bremerhaven, Germany
[d] SIOS-KC - Svalbard Integrated Arctic Earth Observing System Knowledge Centre, Longyearbyen, Norway
[e] Norwegian University of Science and Technology, Trondheim, Norway
[f] UiT the Arctic University of Norway, Tromsø, Norway

ARTICLE INFO

Keywords:
Sea-ice algae
Spectral properties
Bio-optical algorithms
Machine learning
Spectral (un)mixture analysis
Relative ice algal biomass index (RBI)

ABSTRACT

The impact of a rapidly shifting sea-ice cover on climate, ecosystem processes and biophysical habitat properties is not yet fully understood, particularly in the central Arctic Ocean, due to a lack of spatially representative observations. From June to July 2020 during the year-long Multidisciplinary drifting Observatory for the Study of Arctic Climate (MOSAiC, leg 4) in the Transpolar Drift, we deployed an underwater hyperspectral imager (UHI) mounted on a remotely operated vehicle (ROV) to characterize the biophysical properties of different sea-ice habitats. We conducted UHI surveys along two transects: i) under level first-year sea ice (FYI), which had a mean sea-ice draft of 1.4 m and was composed of primarily level FYI but also had a relatively shallow ridge (keel depth ~2.6 m); and ii) under the flank of a ridge, named *Jaridge*, with a mean ice draft of 1.7 m, which was composed of a mix of level ice and thicker ridge blocks with over 3 m draft. We present a new unsupervised bio-optical quantification algorithm for hyperspectral surveys, the relative ice algal biomass index (RBI), using spectral mixture analysis (SMA). We compare this method to the supervised machine learning habitat classification algorithm, Support Vector Machine (SVM). The RBI showed good agreement to literature-based normalized difference indices (NDI) and PCA analyses, which confirm the RBI as a reliable unsupervised index for ice algal biomass. Our biophysical characterization of the two surveyed regions showed an association of sea-ice algal biomass with sea-ice ridge features. Our surveys also indicate that ice algal spatial distribution may be influenced by ice melt rates, and the formation of under ice meltwater layers and false bottoms. With high spatial coverage (>100 m) at microscale resolution (~cm) we documented large spatial variability of summer Arctic sea-ice algal biomass and different patterns between adjacent ice habitats. We further demonstrate the need for improved understanding of sea-ice algal spatial variability as a complementary tool for sea-ice biogeochemical sampling using destructive ice core sampling.

* Corresponding author. Norwegian Polar Institute, Fram Centre, Tromsø, Norway.
E-mail address: benjamin.lange@ngi.no (B.A. Lange).

https://doi.org/10.1016/j.rsase.2024.101224
Received 29 August 2023; Received in revised form 10 March 2024; Accepted 7 May 2024
Available online 8 May 2024

List of acronyms

Acronym	*Full Form*
ANOVA	Analysis of Variance
EOF	Empirical Orthogonal Function
EM1	Endmember 1
EM2	Endmember 2
FCLS	Fully Constrained Least Squares
FOV	Field of View
FYI	First-Year Ice
LBL	Long Baseline
MYI	Multiyear Ice
NDI	Normalized Difference Indices
NPP	Net Primary Production
PAR	Photosynthetically Active Radiation
PCA	Principal Component Analysis
PDF	Probability Density Function
QGIS	Quantum GIS
RBI	Relative Ice Algal Biomass Index
ROI	Region of Interest
ROV	Remotely Operated Vehicle
SMA	Spectral Mixture Analysis
SVM	Support Vector Machine

1. Introduction

Warming of the global climate is causing dramatic shifts in Arctic sea-ice habitats through thinning and the loss of established thick, old multiyear ice (MYI) (Kwok 2018; Stroeve and Notz 2018). These include shifts in the mobility of the pack ice with consequences for formation and distribution of unique sea-ice habitat features, such as pressure ridges (Itkin et al., 2017; Wadhams and Toberg 2012). The impact of these changes on climate, ecosystem processes and biophysical habitat properties is not yet fully understood, particularly in the central Arctic Ocean (Gerland et al., 2019). In the Central Arctic, where sea ice can still persist year-round, sea-ice algal productivity can contribute up to 60% of summertime net primary production (NPP) (Fernández-Méndez et al., 2015; Gosselin et al., 1997; Matrai and Apollonio 2013), while the contribution is lower in the surrounding continental shelf regions (e.g., Arrigo and van Dijken 2015). The presence, spatial distribution and availability of sea-ice algae is of critical importance to Arctic food webs because they provide a concentrated energy resource for under-ice grazers before the onset of significant pelagic production (e.g., Kohlbach et al., 2016; Wang et al., 2015). Thus, understanding the biophysical habitat properties that control the spatial distribution, timing and availability of ice algal biomass (Katlein et al., 2014) is essential to understanding how continued changes to sea-ice habitats will impact Arctic foodwebs (e.g., Lannuzel et al., 2020; Søreide et al., 2010).

Strong seasonality and a variable wind-driven distribution of snow on sea ice drives significant spatio-temporal variability in the accumulation of algae within sea ice (e.g., Lange et al., 2019). Furthermore, other physical drivers such as brine channels and microscale crystal structure of the bottom ice skeletal layer have also been shown to influence the spatial distribution of ice algae (e.g., Cimoli et al., 2020; Lund-Hansen et al., 2016). Yet, the number of studies focusing both on spatial and temporal variability of sea ice are sparse and logistically demanding, but they are nevertheless necessary for accurate characterization of sea-ice habitat quality and quantity across the Arctic and polar seas (Miller et al., 2015). Sea-ice coring has been the standard sampling method for biogeochemical sea-ice studies (Miller et al., 2015). However, it is difficult to achieve a spatially representative sea-ice sample from ice coring alone (Lange et al., 2017b). Furthermore, ice coring is destructive, consequently making temporal studies challenging. Improved technologies are required to overcome limitations intrinsic to existing sea-ice sampling techniques and to bridge some of the spatio-temporal gaps in our understanding of sea-ice bio-physical and biogeochemical processes.

Bio-optical algorithms have been developed to retrieve ice-algal biomass from under-ice cosine corrected hyperspectral irradiance measurements (Campbell et al., 2014, 2015; Melbourne-Thomas et al., 2016; Mundy et al., 2007; Wongpan et al., 2018). Similar algorithms have been developed and applied to cosine-corrected sensors mounted on remotely operated vehicles (ROV) (Lange et al., 2016; Meiners et al., 2017) and under-ice profiling platforms (Lange et al., 2017b) to capture algal biomass variability at spatial scales from meters to kilometers. However, these applications make use of spectroradiometers, which capture light reaching one point and a footprint between 0.5 and 10 m (depending on the FOV and the distance of the sensors from the ice/ocean interface) without providing much information on the spatial distribution of the light field, particularly at sub-meter scales. Hyperspectral imaging can overcome this limitation while maintaining non-destructive functionality. Due to technological constraints, it is only recently that underwater hyperspectral imagining (UHI) systems have been available for underwater marine applications (Cimoli et al., 2017; Johnsen et al., 2013; Mogstad et al., 2019). Polar marine applications of UHI have appeared in the literature over the past few years with use for mapping Arctic macroalgae in a Svalbard fjord (Summers et al., 2022), and deployments under Antarctic sea ice for mapping biophys-

ical sea-ice properties (Cimoli et al., 2019) and ice algal biomass (Cimoli et al., 2020). Cimoli et al. (2020) deployed an UHI onboard an under-ice sliding platform for mapping Antarctic ice algal biomass at unprecedented spatial scales between 1 mm and 20 m. Cimoli et al. (2020) have significantly advanced the possibilities for sea-ice algal observations using UHI systems by demonstrating the reliability of several bio-optical algorithms, which can be applied to UHI surveys for mapping ice algal chlorophyll *a* (chl *a*) biomass. Most of the bio-optical algorithms presented by Cimoli et al. (2020) require ice core extraction and pigment analysis for robust calibration and validation (cal/val). However, they have also demonstrated that principal component analysis (PCA) as a reliable proxy for ice algal biomass without the need for cal/val ice core pigment data. While Lange et al. (2016) also demonstrated that Empirical Orthogonal Function analysis (EOF, also known as PCA) was a more robust bio-optical algorithm for highly varying sea ice and snow conditions (i.e., light field) when applied to hyperspectral irradiance point measurements. Cimoli et al. (2020) present a robust analysis of UHI surveys from level, landfast Antarctic sea ice with no snow cover and a relatively uniform light field. The usability of these bio-optical methods for UHI systems requires further investigation under more variable sea ice and snow conditions and in different regions with perhaps different algal community composition. For example, sea-ice ridges and thick undulating hummock features have been identified as potential ice algal hotspots (Fernández-Méndez et al., 2018; Lange et al. 2017a, 2017b), but sampling these really thick features poses great logistical constraints, thus requiring alternate observation approaches to better understand their contribution to polar ecosystems.

ROVs enable large, floe-scale (100s of meters) surveys and more flexibility in survey design, particularly, to survey undulating under-ice topography and highly varying sea-ice features (e.g., ridge keel blocks), which may not be possible with under-ice L-shaped arms or sliding platforms (Cimoli et al. 2019, 2020; Lange et al. 2016, 2017b). Integration of UHI systems on ROVs have been documented (Dumke et al., 2018a; e.g., Mogstad et al., 2020; Summers et al., 2022) for shallow and deep-sea benthic surveys, however, ROV-UHI surveys of sea ice are not yet available in the literature.

Here we present the novel integration of a UHI system onboard a ROV for the purpose of mapping spatial-temporal variability of biophysical sea-ice properties and sea-ice algal biomass in the Central Arctic Ocean. This is the first study of Arctic sea ice using a UHI mounted on a ROV. Surveys were conducted over a 1-month summer period (June to July 2020) during the year-long Multidisciplinary drifting Observatory for the Study of Arctic Climate (MOSAiC). Due to the nature of the site setup of the MOSAiC Central Observatory (the main ice floe with all sampling and survey locations), no destructive sampling was to be conducted within the ROV main survey site, thus limiting the possibility for collocated ice coring pigment analyses necessary for traditional bio-optical algorithm development and cal/val (Montes-Herrera et al., 2021). Thus, we aimed to assess different methods for the biophysical characterization of sea-ice habitats using UHI without the need for logistically demanding ice core samples. Using the most reliable method, we characterize the biophysical properties of the surveyed areas.

2. Materials and methods

2.1. Study area and survey overview

We present observations made using a UHI mounted on a ROV. Surveys were conducted below the first-year sea ice (FYI) region within the Central Observatory (CO) during leg 4 (June to July 2020) of MOSAiC (Nicolaus et al., 2022). For the purposes of UHI surveys, we had two regions of interest: an area of level ice and an area along the flank of a sea-ice ridge, *Jaridge* (Lange et al., 2023). We conducted a total of 10 UHI surveys over a one-month period, five surveys within the level ice area and five surveys along the ridge flank (Fig. 1). Here we present only one set of surveys conducted on July 01, 2020 between 14:30 and 15:00 UTC (i.e., one from level ice and one from the ridge flank).

The ROV surveys were conducted with an Ocean Modules M500. Operation and sensor configurations (excluding the UHI) followed (Katlein et al., 2017). This same ROV system has been used extensively for under-ice bio-optical surveys (Campbell et al., 2022; Katlein et al., 2019; Lange et al., 2019), however, this was the first use with a hyperspectral imager onboard this ROV and in the Arctic Ocean. The ROV position was determined using long baseline (LBL) acoustic positioning with an accuracy on the order of 0.5 m. ROV-UHI surveys were conducted with a target distance of 1–2 m between the UHI sensor (top of the ROV) and the ice bottom wherever possible. Navigating along the ridge flank was difficult due to the highly variable ice bottom topography (e.g., ice draft ranging from 1.5 to 6 m) and thus resulted in more fluctuations in the distance between the ROV and ice bottom.

The UHI system used during these surveys was an Ecotone UHI model 4 (Ecotone AS, Trondheim, Norway) line scanner, rated to 2000 m water depth. The sensor has a 60° field of view (FOV) in the transverse direction (across track) and ~0.4° FOV longitudinal direction (along track). The across track spatial resolution is 1936 pixels with a binning of 2 resulting in processed images of 968 pixels. The edges of the images were cropped, due to spectral noise, to a final along track dimension of 778 pixels. This resulted in mean ± sd across-track image swath widths (at the ice bottom surface) of 1.29 ± 0.48 m (range 0.24–2.43 m), for the ridge flank survey, and 1.00 ± 0.26 m (range 0.12–1.79 m) for the level ice. Correspondingly, mean pixel widths were 1.7 and 1.3 mm, respectively, and a range of 0.15–3.1 mm over both surveys. The spectral range is 381–749 nm, with 214 spectral bands and a spectral resolution of ~1.7 nm. The system was integrated to the ROV onboard and was mounted so that the top of the camera was flush with the surface of the ROV (Fig. 2) and to maintain proper along track and across track scanning orientation with the direction of travel. The UHI integration allowed live data and video feeds to the ROV operation computer during surveys. Thus, spectral quality and features could be assessed and noted in real time. During initial test surveys we determined the optimal integration time to be 40 ms based on the real time assessment of the spectral quality under both ice types, level ice and ridge flank. The UHI was used to capture transmitted radiance, using no artificial light sources.

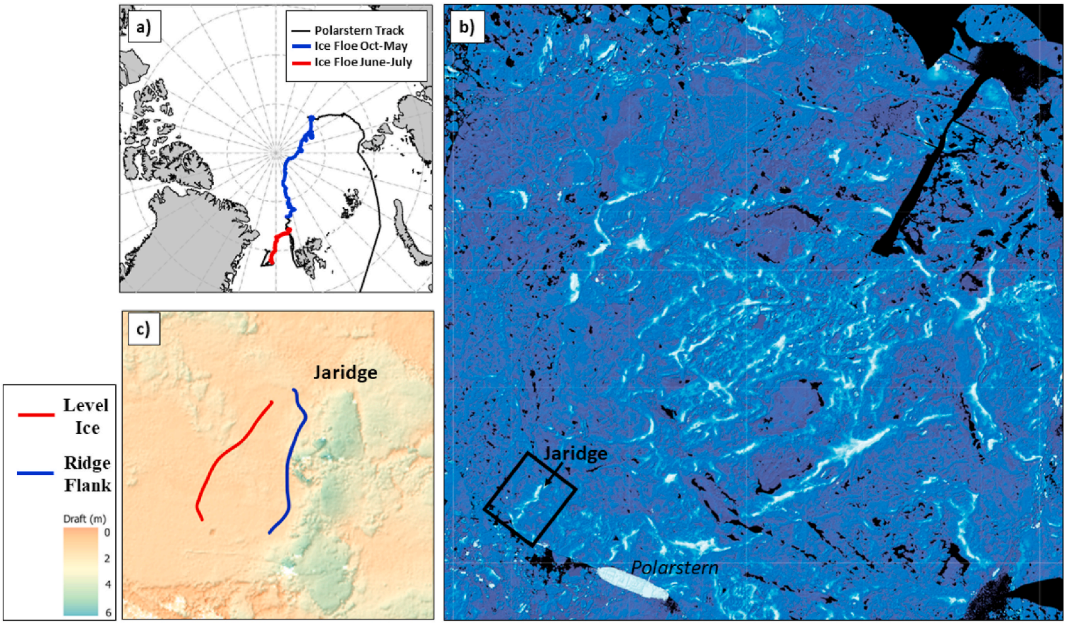

Fig. 1. a) overview of MOSAiC ice floe drift and Polarstern track; b) airborne laser scanner surface topography map of the MOSAiC ice floe from July 01, 2020 (for scale, Polarstern is 118 m in length); c) Multibeam sonar sea-ice draft map of the study site showing the two UHI survey transects (dark blue is low elevation, white is high elevation).

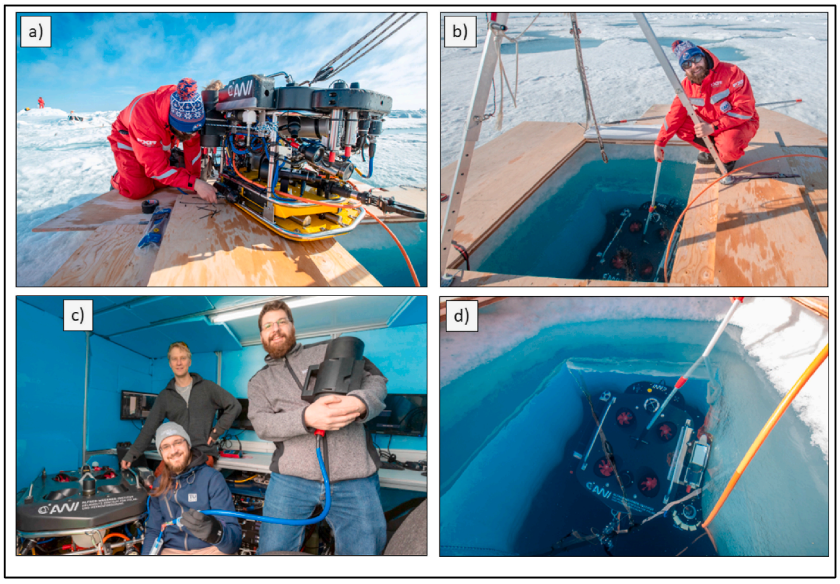

Fig. 2. Pictures of the Underwater Hyperspectral Imager integration with the Remotely Operated Vehicle. A) B. Lange adjusting ROV buoyancy in the field before deployment. b) Careful deployment and submersion of the ROV under the ice. c) ROV-UHI integration team testing cable connection inside the ROV hut. d) Top view of the ROV with the upward looking UHI shown in the bottom right of the ROV.

2.2. Spectral processing

An overview of the processing steps is depicted by a flowchart in Fig. 3. Radiometric processing was conducted using the manufacturer provided software, 'Immersion', including the manufacturer's internal calibration parameters. All subsequent processing and analyses were conducted in Python 3 and QGIS 3.24 by combining both the level ice and ridge flank surveys into one dataset. We combined the datasets to increase the variability of environmental conditions included in bio-optical model development while also minimizing any potential bias, which could be introduced due to unique properties of the selected surveyed regions or regions of interest (ROIs). This also increased the sample size and increased spectral variability resulting in more robust models able to cover a larger range of environmental conditions.

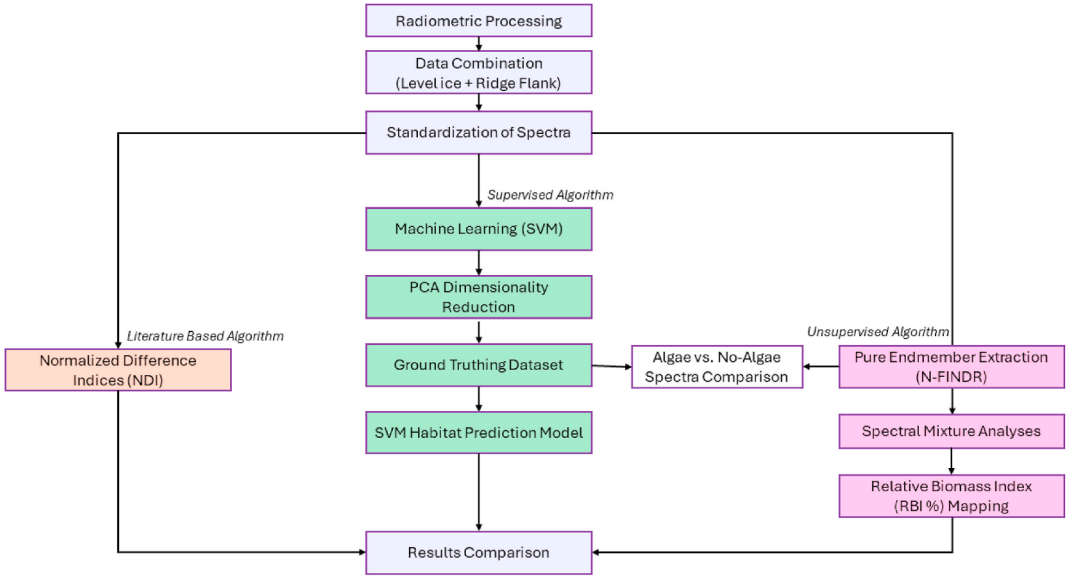

Fig. 3. Flowchart diagram showing the processing and analytical steps and methods used in this study.

Each radiance spectrum was standardized by subtracting the mean of the spectrum then dividing by the standard deviation of the spectrum (Lange et al., 2016; Taylor et al., 2013). Standardizing the spectra reduces the variability due to the magnitude of the light intensity and allows for a more detailed examination and comparison of spectral shape (Craig et al., 2012; Taylor et al., 2013). Radiance and standardized spectra are shown in Fig. 4 a and b demonstrating how it is difficult to assess and compare spectral shape when there is large variation in magnitude. Here the example given is spectra extracted along a transect from a low/no algae region (An inset Fig. 4 a) and into the middle of an algae patch (B inset Fig. 4 a) (i.e., crossing a gradient of algae biomass).

2.3. Supervised classification with machine learning

Here we used a machine learning approach for habitat classification called Support Vector Machine (SVM) (Freitas et al., 2021) implemented using Python *sklearn*. The first step was to reduce the dimensionality of the large spectral dataset by applying a PCA on the combined (level and ridge flank) standardized survey spectra. The first nine PCs were kept for further analyses.

The next step was to create a ground truthing dataset for the supervised classification. The ground truthing dataset includes image pixels with classes 'Algae' and 'No-Algae'. This was accomplished by manually inspecting and identifying regions with Algae and No-Algae within RGB image composites to delineate the regions of interest (ROI) for the two classes: 1. Algae (ie., suitable algae habitat); and 2. No-Algae (ie., not suitable algae habitat). RGB composite images (from UHI surveys) were exported into QGIS and manually inspected. A blank raster file was imported into QGIS to populate with the ground truthing class values. ROIs were delineated on the RGB images and the corresponding raster pixels from the class raster were assigned the appropriate class values: 1. Algae or 2. No-Algae. The ground truthing raster file was then imported in python to extract the spectra for each corresponding class. Fig. 5 shows an example of the RGB image, selection of ROIs and their corresponding spectra. All analyses were conducted on images without georeferencing (ie., no spatial scale or information associated with the image).

Spectra were extracted from each ground truth class and combined with the PCA analyses to create an optimal SVM habitat prediction model. SVM is a common habitat classification method applied to underwater (Chennu et al., 2017; Dumke et al., 2018b; Summers et al., 2022) and airborne hyperspectral imagery (Tait et al., 2019). The SVM model cross validation provided important information on the predictive power of the developed habitat classification model. The SVM model was then applied to the entire UHI survey (including both the level and ridge flank surveys).

2.4. Unsupervised classification using spectral mixture analyses

Spectral mixture (unmixing) analyses was used to identify 'pure' spectral endmembers, which could be used for extreme ends of the algal biomass spectrum (i.e., no algae vs 100% algae biomass). The end result of the SMA was the classification of each pixel's spectrum as a percent mixture of the two endmember spectra, representing the percent relative sea-ice algal biomass for the surveyed regions, which we have termed the Relative sea Ice algal Biomass index (RBI, %). The spectral mixture analyses, and developed RBI, method was applied to estimate the quantity of algae biomass rather than discriminate or classify the algae. We applied the automated N-FINDR endmember extraction algorithm, using the Python's *pysptools* package and associated Endmembers Extraction Algorithms (EEA), setting $N = 2$ endmembers (i.e., no-algae and 100% algae) (Ji et al., 2015). The resulting two endmember spectra are shown in Fig. 4e and show similarities to the manually selected no-algae and algae spectra confirming the use for the RBI. Using the selected endmember spectra, we created RBI (%) maps of the entire survey data using the fully constrained least squares (FCLS) linear spectral mixture analysis method.

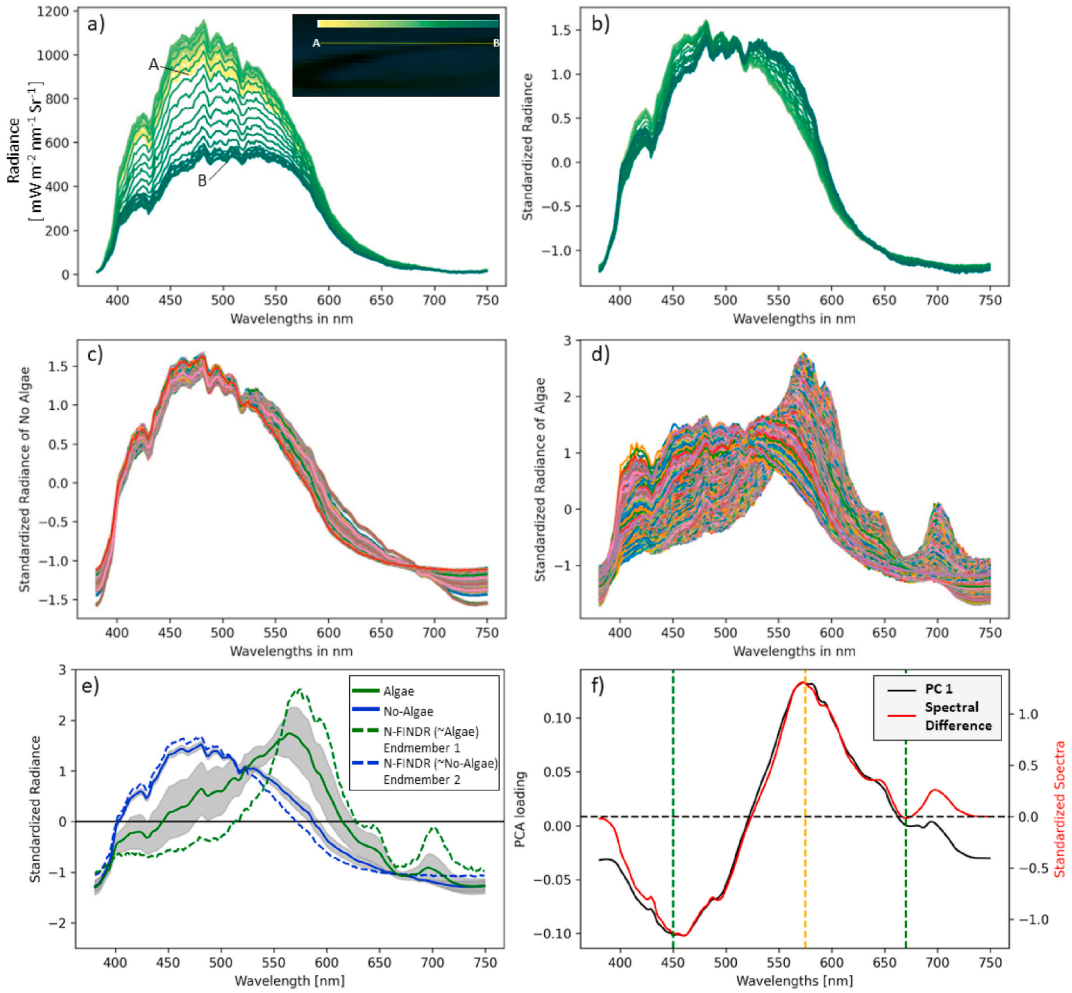

Fig. 4. Comparison between a) processed radiance spectra and b) standardized spectra along transect from no algae into the center of an algae patch (inset A to B, respectively); c) no algae spectra (N = 10,254); d) algae spectra (N = 22,925); e) mean of no-algae and algae spectra from c and d, respectively, and the difference between the two spectra (standard deviation shown as grey shaded area); f) spectral difference between mean algae and no-algae (right y axis) combined with PCA-1 loadings (left y axis, i.e., mode of oscillation) the vertical dashed green lines indicate approximate locations of chl *a* peak spectral absorption (approx. 450 and 670 nm) and vertical yellow line indicates the maximum difference between spectra at approx. 575 nm). (For interpretation of the references to color in this figure legend, the reader is referred to the Web version of this article.)

2.5. Literature-based spectral indices

We applied normalized difference indices (NDI) to the standardized spectra using wavelength combinations from previous Arctic (490:478 nm) (Campbell et al., 2014) (683:669 nm) (Lange et al., 2016) and Antarctic studies (517:449 nm) (Cimoli et al. 2019, 2020). We also investigated the different principal components (PC) as proxies for ice algal biomass (Cimoli et al. 2019, 2020; Lange et al., 2016). The results from the literature-based NDIs, PCA, SVM and RBI were compared and investigated to test their utility under such variable environmental conditions.

3. Results and discussion

3.1. Sea-ice thickness and transmitted irradiance

The ridge flank survey area, overall, was thicker than the level ice survey area (Table 1; Fig. 6) but also consisted of some level ice that was comparable to the larger scale mean level FYI draft of 1.40 m measured using the ROV multibeam sonar observations from July 01, 2020 (Salganik et al., 2023). The level ice had one region of thicker ice, which was a relatively thinner ridge named '*Porridge*' (Fig. 1; Fig. 6). The predetermined ice habitat classes of the UHI surveys were a mix of both level ice and ridges, thus, complicating the original survey design for a simple ice type/habitat comparison between the surveyed areas. Thus, when we examine both surveys, 'level FYI' and 'ridge flank', we must keep in mind that they both represent a mix of ice types. Because of the thicker sea ice, the ridge flank had lower overall transmitted light levels with mean ± sd integrated irradiance of 1.45 ± 1.02 W m^{-2} compared to level ice of 1.69 ± 1.10 W m^{-2} (Table 1). The ridge flank was also influenced by large snow accumulation along the surface flanks of the

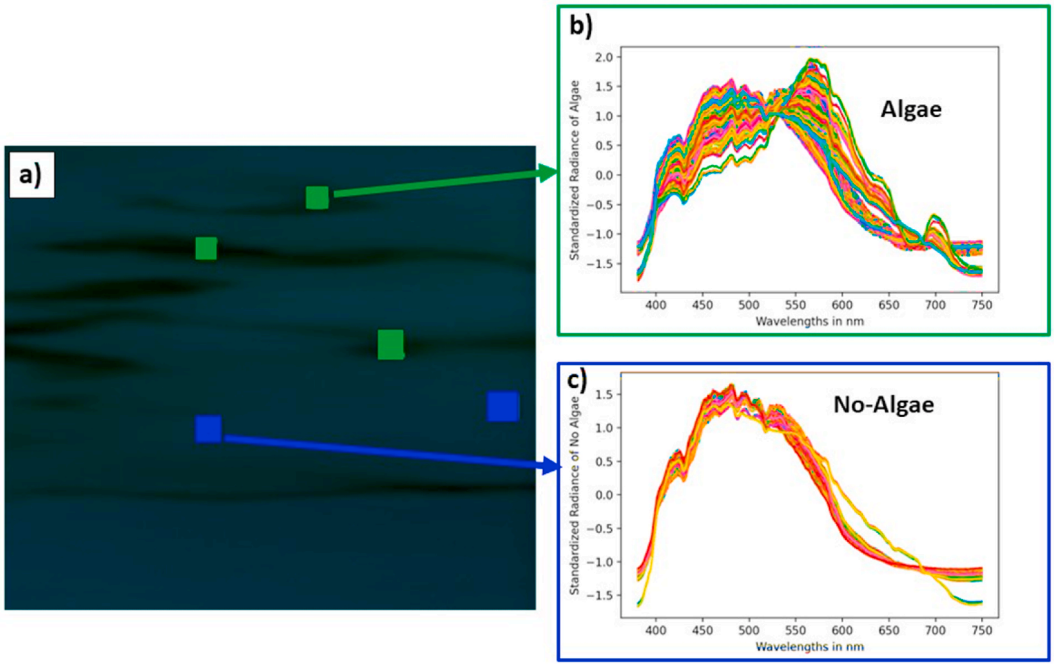

Fig. 5. Example of the delineation of the region of interests (ROIs): a) showing a RGB composite (x, y axes are simply row and column with no spatial information) image with selected ROIs for the two habitat classes: algae (green) and no-algae (blue); and spectra from the corresponding classes: b) algae; and c) no-algae.

Table 1
Biophysical summary for each UHI survey area. Ice draft taken from multibeam sonar surveys on June 29, 2020.

	Level ice area	Ridge Flank area
Ice draft (m) (mean ± sd)	1.39 ± 0.30	1.74 ± 0.44
Integrated Irradiance (PAR) W m^{-2} (mean ± sd)	1.69 ± 1.10	1.45 ± 1.02
Relative Biomass (mean ± sd)	0.13 ± 0.10	0.11 ± 0.05
Suitable Algae Habitat	9 %	24 %

ridge sail that stayed well into advanced melt season (Lange et al., 2023). The UHI provides an advantage over typical radiometers because it captures this variability on small scales, which is likely important for algae biomass distribution and an improved understanding of the relationship between sea-ice algae and radiative transfer on small spatial scales (e.g., mm).

3.2. Spectral properties

Fig. 4 a and b demonstrate that it is easier to observe the variation in the shape of standardized spectra because of changes in algal biomass across a transect compared to the processed radiance spectra, which include additional variability resulting from the amount of light (i.e., the magnitude of the spectra). Thus, confirming the use of standardized spectra for further analyses. Algae are photosynthetic organisms and thus have pigments that absorb light in different spectral ranges including the Photosynthically Active Radiation (PAR) wavelength range from 400 to 700 nm. Removing the influence of light magnitude on spectral variability reduces the chance of introducing bias into the model or an artificial relationship (Lange et al., 2016; Taylor et al., 2013).

Spectra from the manually identified classes (ROIs): 1-algae and 2-no-algae showed strong similarities with their corresponding 'pure' endmember spectra, which were automatically identified from the entire UHI survey dataset (level and flank combined; Fig. 4 e) using the N-FINDR algorithm. There was also similarity between the spectral difference of the mean algae and no-algae compared to the mode of oscillation for the first principal component (PCA 1; Fig. 4 f). These are independent methods, one manual and one computational, providing a robust and thorough assessment of the spectra that demonstrates excellent comparability between these two methods.

3.3. Comparison between Support Vector Machine and relative ice algal biomass index

Cross-validation of the SVM model showed highly reliable predictability, with an accuracy of over 99%, given the training dataset and model parameters (Fig. 9). The similarity of the mode of oscillation (ie., explained variance of PC1 over the spectral wavelength range) with the difference spectrum from the mean algae minus the mean no-algae spectra further emphasized that PC1 as a good biophysical parameter for explaining the variability of algae. Furthermore, visual inspection of the SVM habitat classification showed

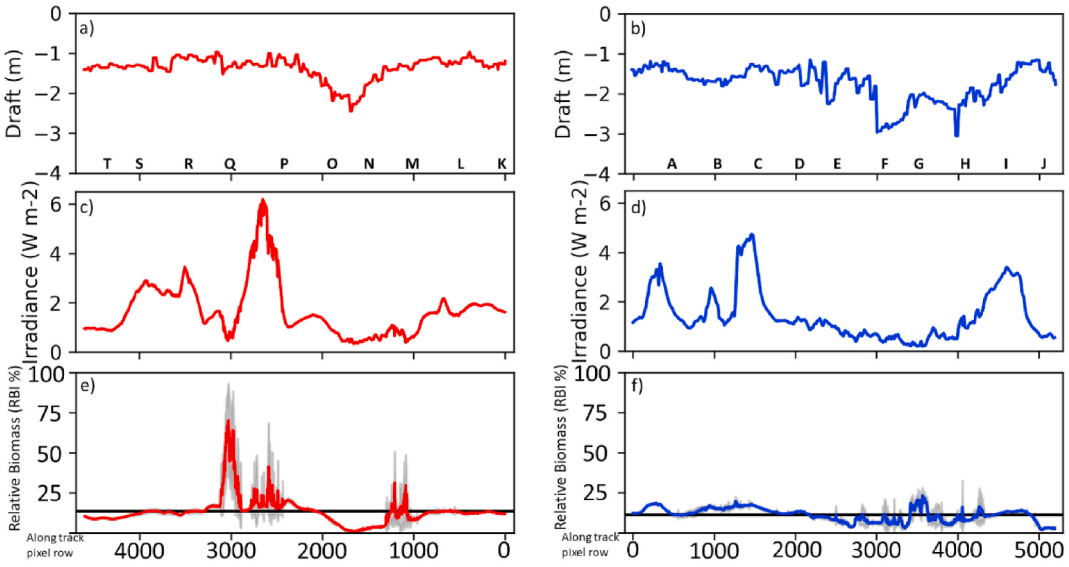

Fig. 6. Horizontal profiles along the level ice (red, left panels) and ridge flank (blue, right panels) UHI surveys: a) and b) ice draft; c) and d) transmitted irradiance; and e) and f) across-track mean relative ice algal biomass (RBI - %) (grey shaded area represents ± one standard deviation). (For interpretation of the references to color in this figure legend, the reader is referred to the Web version of this article.)

good agreement between areas with visible algae aggregates and regions classified as suitable algae habitat (ie., class = 'Algae') (Fig. 7 c-f). Visual inspection comparing the RGB composites with the relative biomass also showed that the areas where large algae aggregates were located also had the highest relative biomass (Fig. 7 c-n and Fig. 8 c-n). Nevertheless, it is difficult to assess on the full survey scales how well the SVM model is at classifying regions of lower biomass because these regions are also less obvious based solely on visual inspection of RGB composites. This perhaps is one limitation of using manual visual identification of algae as a training dataset and may produce underestimates of algae habitat since low biomass regions may not be included in the training dataset.

The two N-FINDR endmember spectra agreed well with the mean algae and mean no-algae spectra (Fig. 4 e). The first endmember (EM1) had a similar shape as the algae spectrum but was outside the standard deviation (Fig. 4 e). The algae spectra showed large variability (Fig. 4 d) and the endmembers are by definition extreme values, thus it stands to reason that the EM1 spectrum was outside the standard deviation of the mean algae spectrum and towards the extreme values as shown in the algae spectra (Fig. 4 d). Whereas the second endmember (EM2) was nearly identical to the no-algae mean spectrum (Fig. 4 e), which was expected since there was low variability within the no-algae spectra (Fig. 4 c). This provides confidence in the assignment of EM2 and EM1 spectra as endmember representatives of 0 and 100% relative ice algal biomass, respectively.

Despite having good agreement between the mean algae spectrum and EM1 spectrum, and between the mean no-algae spectrum and EM2 spectrum, there was some discrepancies when comparing the SVM habitat classification and relative biomass. First, SVM showed higher spatial coverage of suitable algae habitat for the ridge flank at 24% compared to level ice at 9 % (Table 1) whereas the mean RBIs were similar for each survey at 13 ± 10 % and 11 ± 5 %, respectively (Table 1). The probability density function (PDF) plots of RBI (Fig. 10) showed there were significantly larger portions of the level ice with nearly zero or very low RBI and substantial regions of high RBI (Fig. 10). This pattern was obvious for the high RBI regions when inspecting the spatial maps, however, less obvious for low RBI (Fig. 6). The spatial distribution of RBI were quite different between the two surveyed regions, however, the overall mean RBI were the same. Discrepancies between SVM and RBI approaches are further evident within the PDFs of relative biomass divided into the different SVM habitats (algae and no-algae) and for the different ice types. There appears to be some difference/bias in how the SVM model assigns suitable algae habitat between the two different ice habitats. This difference could be related to the limitation of identifying low biomass regions as suitable algae habitat for the training dataset, thus also introducing a bias in the SVM suitable habitat classification for low biomass regions. There is more overlap of RBI values between the two habitat classes for the ridge flank survey (Fig. 10). This perhaps indicates an overestimation of suitable algae habitat, in addition to (or instead of) an underestimation of low biomass regions in the level ice survey since there is little overlap in RBI between the two habitat classes for the level ice survey (Fig. 10).

3.4. Spectral indices and ice algal proxies

We observed poor agreement between the RBI and the two NDI combinations 490:478 (Campbell et al., 2014, 2015) and 683:669 (Lange et al., 2016) (Fig. 12 h and j). These two NDIs also showed grainy patterns in the NDI images (Fig. 12 d and f) and poor visual agreement with the RGB composites where dense algal aggregates were apparent (Fig. 12 a). We observed very good agreement between the RBI and NDI 517:449 nm (Cimoli et al., 2020) (Fig. 12 i). The 449 nm wavelength is located at the peak difference between algae vs. no-algae spectra (Fig. 4 e) and the 517 nm wavelength is located near the minimum difference. The 449 nm wavelength is also near the chl *a* absorption peak while 517 is outside the high absorption region, making it a theoretically ideal wavelength combi-

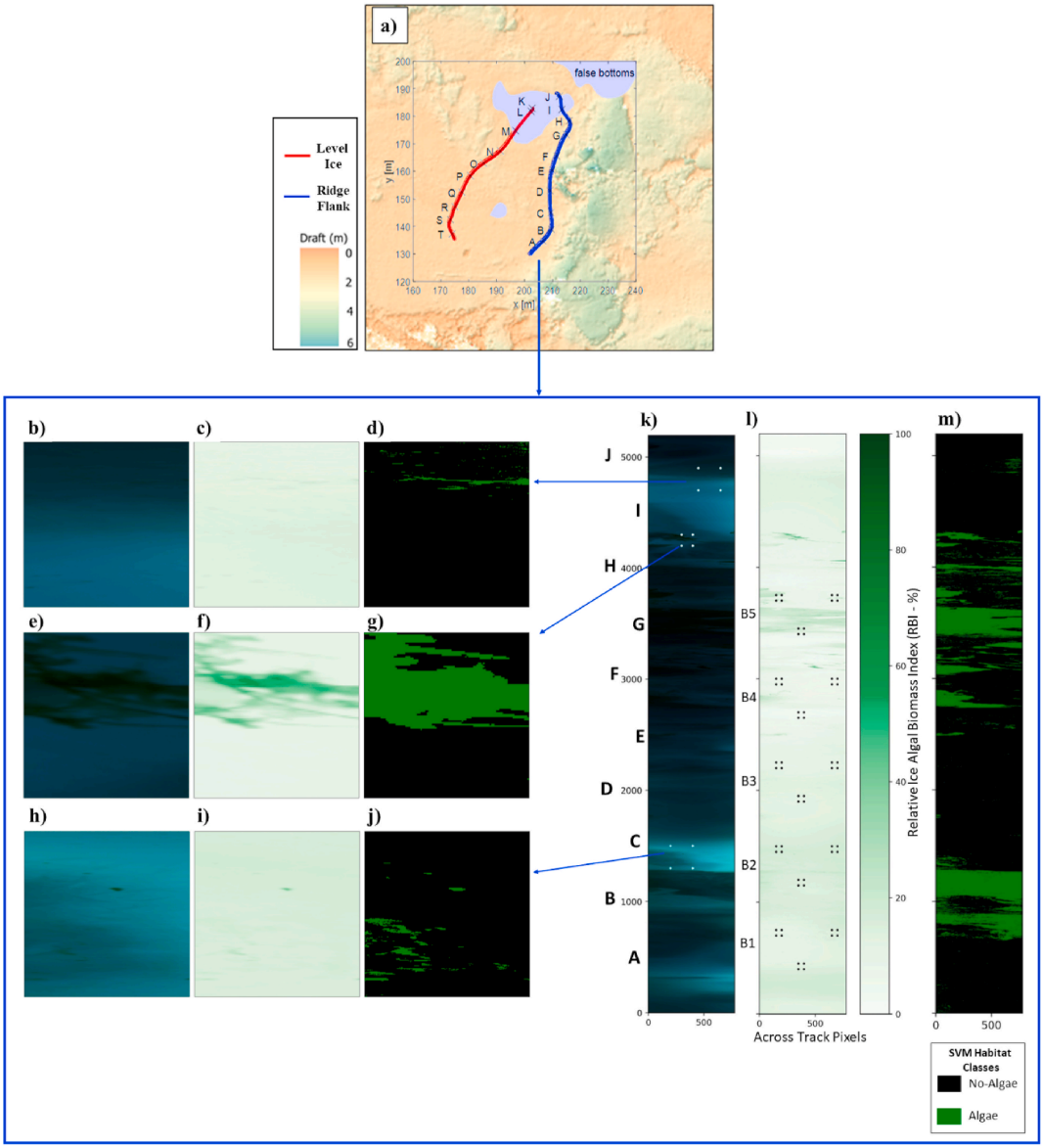

Fig. 7. a) bottom ice topography map (ice draft) showing the UHI survey lines for level ice (red) and ridge flank (blue), with overlaid polygons indicating false bottom areas, and reference points along transects indicated by capital letters with corresponding locations along the ridge flank UHI survey results k), l), and m) NOTE: Across track width dimension (at the ice surface) has a mean of 1.29 ± 0.48 m (range 0.24–2.43 m). Zoomed in regions from corresponding inset (four white points) are shown on: k) RGB composite from the ridge flank UHI survey. b), e) and h) are RGB composites. l) showing Relative Ice Algal Biomass (RBI - %) for the full ridge flank survey with c), f) and i) showing zoomed in regions indicated in k) (four white points). Groupings of 4 black points in l) indicate single hypothetical core locations and each grouping of 3 hypothetical cores is assigned a location B# shown along the left side. m) is the SVM habitat classification map of the full ridge flank survey with d), g) and j) showing zoomed in regions from the corresponding inset in k). (For interpretation of the references to color in this figure legend, the reader is referred to the Web version of this article.)

nation for capturing variability in algal chl *a* biomass (Cimoli et al., 2020). This result suggests the validity of a semi-supervised approach to develop NDI wavelength combinations for ice algal biomass without the need for additional ice core pigment samples. This semi-supervised NDI approach would require visual extraction of algae and no-algae spectra from UHI surveys, as explained in the ground truthing step for the SVM method, examine the difference spectrum and select one wavelength within the peak difference and one near the minimum difference.

Snow is a good absorber of light over 600 nm (Järvinen and Leppäranta 2011; Perovich 1996; Thomas 1963). We observed large variability in snow depth on the ice surface still during mid-summer with large amounts remaining within and along the flanks of sea-ice ridges on the MOSAiC floe (Lange et al., 2023). The combination of high variability in the light field under a large range of snow and ice conditions, such as melt ponds, bare ice, ridge keels, and ice draft between 1 and ~4 m likely had a large influence on the spectral variability, particularly in the higher wavelengths making it more difficult to take advantage of the chl *a* absorption peak around 670 nm, which likely negatively influenced the usability of the NDI combination 683:669 (Lange et al., 2016). Furthermore,

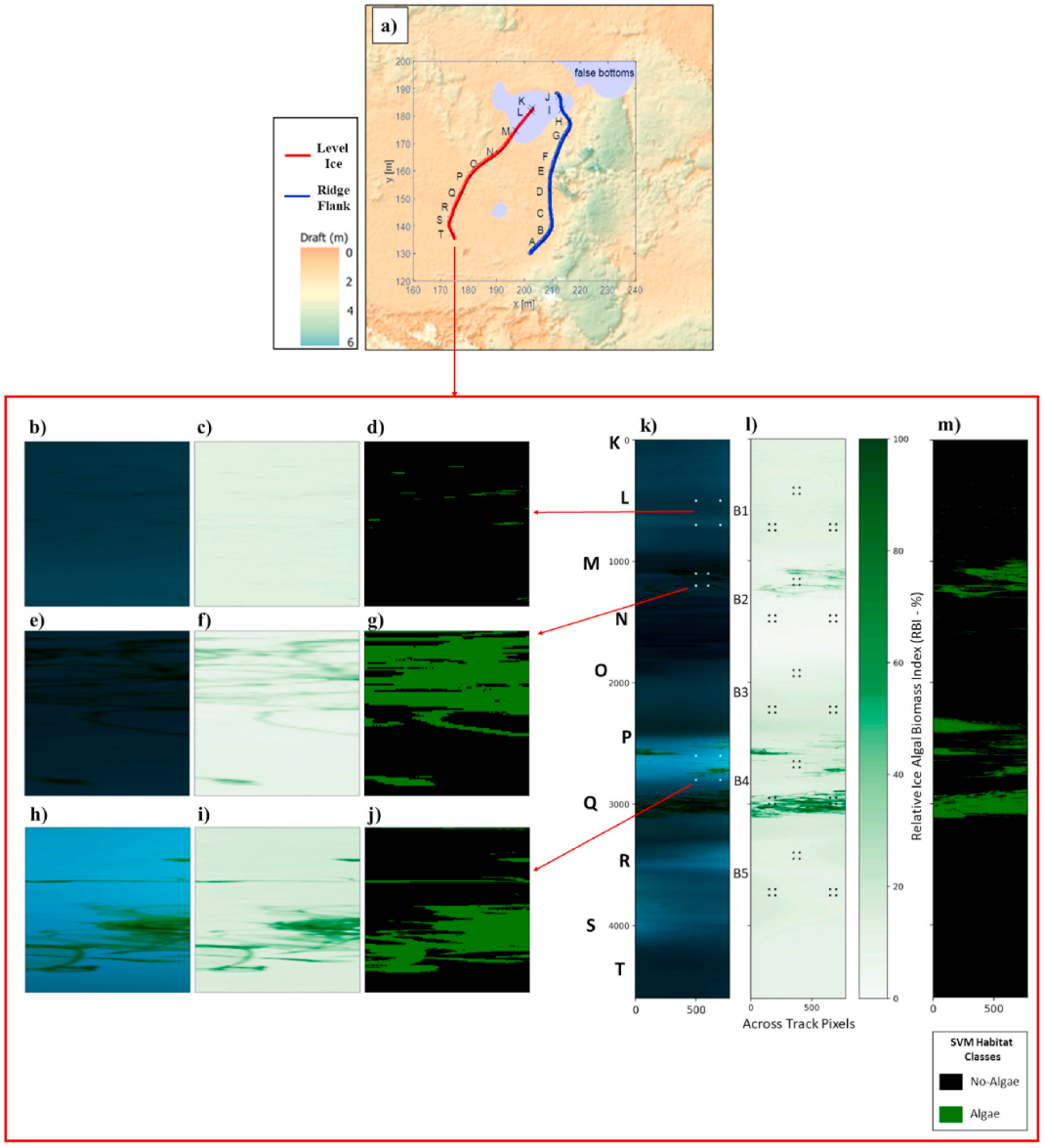

Fig. 8. a) bottom ice topography map (ice draft) showing the UHI survey lines for level ice (red) and ridge flank (blue), with overlaid survey lines and reference points indicated by capital letters with corresponding locations along the level ice UHI survey results k), l), and m) NOTE: Across track width dimension (at the ice surface) has a mean of 1.00 ± 0.26 m (range 0.12–1.79 m). Zoomed in regions from corresponding inset (four white points) are shown on: k) RGB composite from the level ice UHI survey. b), e) and h) are RGB composites. l) showing Relative Ice Algal Biomass (RBI - %) for the full level ice survey with c), f) and i) showing zoomed in regions indicated in k) (four white points). Groupings of 4 black points in l) indicate single hypothetical core locations and each grouping of 3 hypothetical cores is assigned a location B# shown along the left side. m) is the SVM habitat classification map of the full level ice survey with d), g) and j) showing zoomed in regions from the corresponding inset in k). (For interpretation of the references to color in this figure legend, the reader is referred to the Web version of this article.)

there was little difference between the algae and no-algae spectra and no peak in the mode of oscillation for PC-1 in the 650–700 nm range (Fig. 4 f), which further emphasizes the lack of signal in this spectral region. There appears to be a smaller peak in the algae vs. no-algae difference spectrum around 700 nm, which could be explored, however, the 440 nm chl *a* absorption peak has larger variability indicating it is more suitable as a proxy for ice algal biomass. Although the 490:478 NDI combination (Campbell et al., 2014, 2015) is also within the 440 nm chl *a* absorption peak, both wavelengths are near the peak difference between algae and no-algae spectra thus would co-vary with variation in spectral signal and not provide variability in response to changes in chl *a* biomass, which likely caused poor agreement with RBI.

We also observed excellent agreement between RBI and PC-1, with slight deviation in the higher biomass/index region (Fig. 11). The PC-1 showed very good agreement with the difference in endmember spectrum and the difference between the algae and no-algae spectrum (Fig. 4 e and f)). Cimoli et al. (2020) have demonstrated that PCA analyses applied to UHI surveys provides a good unsupervised (ie., without ice core cal/val) proxy for ice algal biomass under relatively uniform light field with level sea ice and no snow

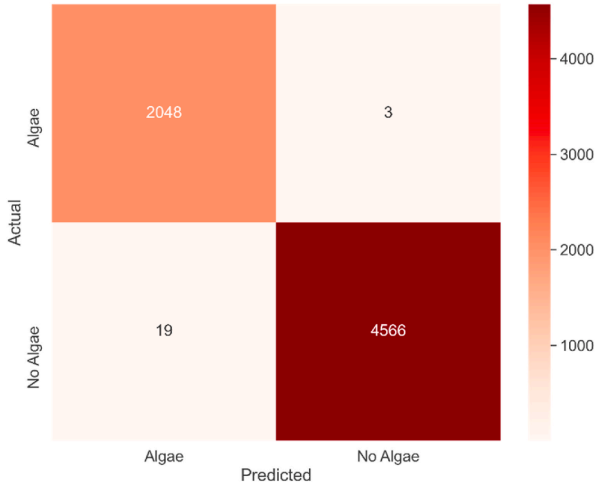

Fig. 9. Confusion matrix of Support Vector Machine model development cross validation.

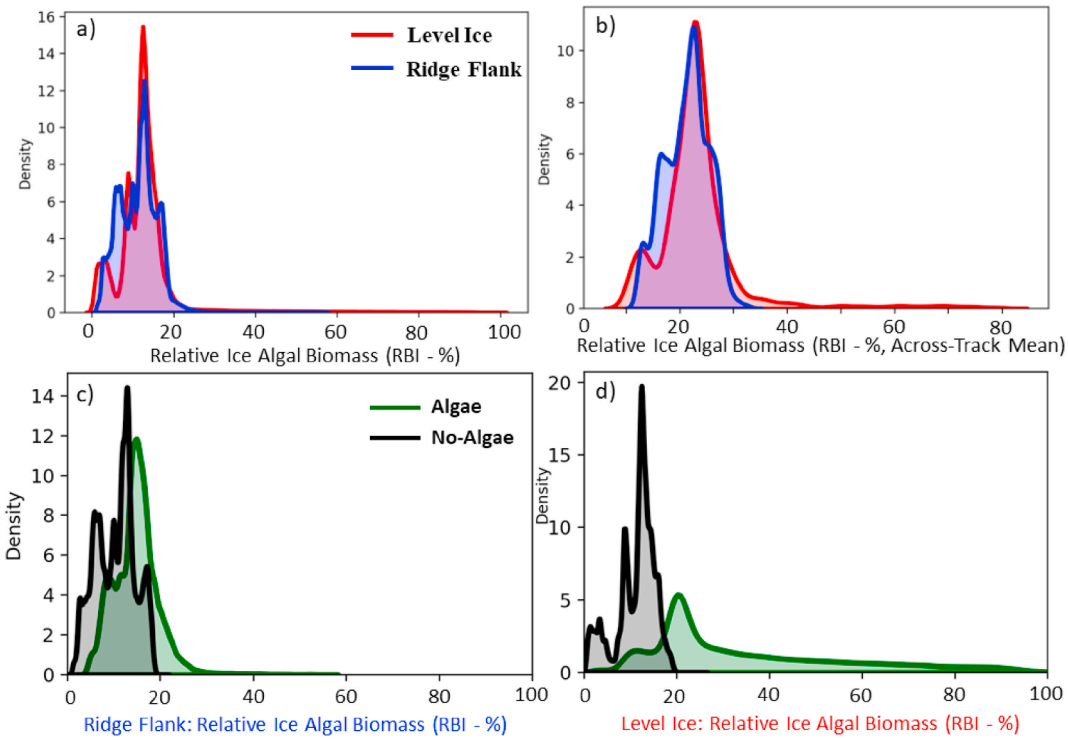

Fig. 10. Probability Density Functions (PDFs) of: a) relative ice algal biomass (RBI - %) per pixel (>7 million pixels) split into the level ice and ridge flank surveys; b) across-track mean (778 pixels) of relative ice algal biomass (RBI - %) split into the level ice and ridge flank surveys. PDFs of relative ice algal biomass (RBI - %) per pixel (>7 million pixels) split into the SVM habitat classes Algae (green) and no-algae (black/grey) for: c) ridge flank survey; and d) level ice survey.

cover. Lange et al. (2016, 2017) have demonstrated the use of PCA/EOF analyses on hyperspectral radiometer surveys (ie., cosine integrated receptors) combined with regression analyses to map ice algal chl *a* biomass under highly variable sea-ice conditions (e.g., different thicknesses, snow conditions, latitudes). Our PCA analyses and comparison to our newly developed RBI and literature-based NDIs confirm the reliability of PCA analyses applied to UHI survey data as a proxy for ice algal biomass. The excellent agreement between the PCA and RBI demonstrate both approaches are suitable as proxies for mapping ice algal biomass under highly varying light conditions. We note that further calibration and validation of these methods with ice core pigment information would be beneficial. However, proxies for algal biomass are sufficient in quantifying spatial and temporal variability at unprecedented spatial and temporal scales, which is severely lacking in sea-ice studies.

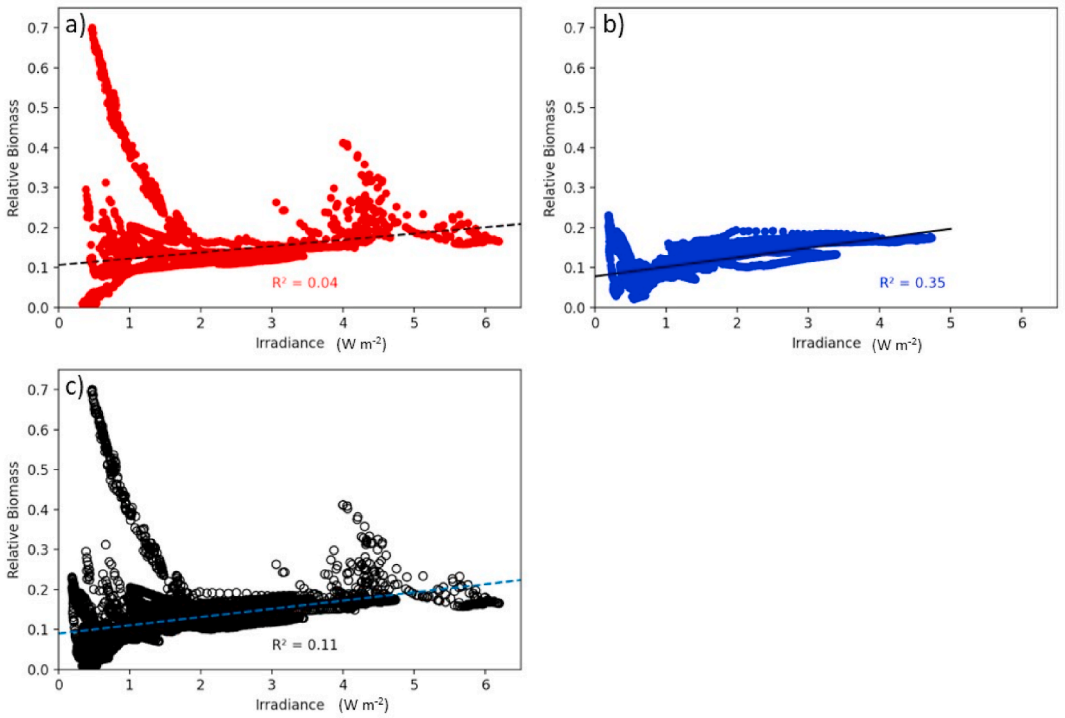

Fig. 11. Scatterplots of across-track mean relative biomass vs. irradiance (integrated across track) for: a) the level ice survey, b) the ridge flank survey, and c) combined. Note the r-squared is shown in each plot for the linear regression lines.

3.5. Biophysical characterization

The SVM habitat classification had some bias in the prediction output likely introduced from the visual identification and extraction of training spectra for the two habitat classes. Nevertheless, the selection of the algae and no-algae training datasets provided important information on the spectral shape of high algae vs. no or very low algae regions. This information helped confirm the automated endmember spectra determination used for the spectral (un)mixture relative ice algal biomass index (RBI) and comparison with literature-based NDIs and PC-1 ice algal proxy. Due to the good agreement of the RBI with both the literature-based NDI combination 517:449 nm (Cimoli et al., 2020) and PC-1 we focus primarily on the RBI results for further biophysical characterization of the two survey regions.

Correlations of irradiance with across-track mean RBI was moderate for the ridge flank (0.59, $p < 0.05$), low for level ice (0.20, $p < 0.05$), and low for all combined (0.33, $p < 0.05$). The overall positive relationship with irradiance indicates ice algae preferentially accumulated in comparatively high light environments. However, there are some obvious negative trends between the RBI and irradiance superimposed on the overall positive trend (Fig. 11). These point groupings with a negative trend are also the regions with highest RBI (e.g., high density algae aggregates), indicating the negative impact of algae on light transmittance due to light absorption (Legendre and Gosselin 1991). This is also obvious within the irradiance and relative biomass profiles (Fig. 6 c and e, respectively) where you see a drop in irradiance at the same location of maximum or peaks in RBI.

We observed a relationship between quality of ice algae habitat and ridge features. On each side of *Porridge,* in the level ice profile, is where the largest regions of SVM suitable algae habitat are located (Fig. 7 c, around labels ~ M and Q), and the highest RBI also with the highest variability (Fig. 6 a and e, pixels ~3000 and ~1000). In the ridge flank profile, there also appears to be high RBI and high variability within or between thick ridge features (Fig. 6 b and f, labels F, G and H and between pixels 3000–4000). There is another region with high RBI variability also with a larger region of suitable algae habitat, which is in close proximity to a ridge block feature but this is only visible from the areal map of ice draft (Fig. 7 a, between labels A-B and around pixel 1000), however, not so apparent from the horizontal ice draft profile (Fig. 6 b). This is in agreement with other studies where (Katlein et al., 2014) showed algal aggregates accumulating in relation to ridges and topographic features, which created shelter from strong ocean currents. Furthermore, (Fernández-Méndez et al., 2018; Lange et al., 2017b) provided observations of algae within sea-ice ridge keels and within the block networks.

We observed the lowest relative ice algal biomass in the ridge flank survey near the end of the transect where a false bottom was also identified (Salganik et al., 2023) (Fig. 7b). False bottoms form when freshwater accumulates under the sea ice and freezes at the interface between the fresher melt water and underlying seawater (Smith et al., 2022). The spatial distribution of freshwater and presence of false bottoms are primarily driven by bottom ice topography (Smith et al., 2022) with freshwater accumulating under the sea ice and in the adjacent leads. The formation of false bottom ice was observed during June and July on the MOSAiC floe (Salganik et al., 2023; Smith et al., 2022) with some patches within the UHI surveys (Figs. 7 and 8). The low salinities characterizing locations of

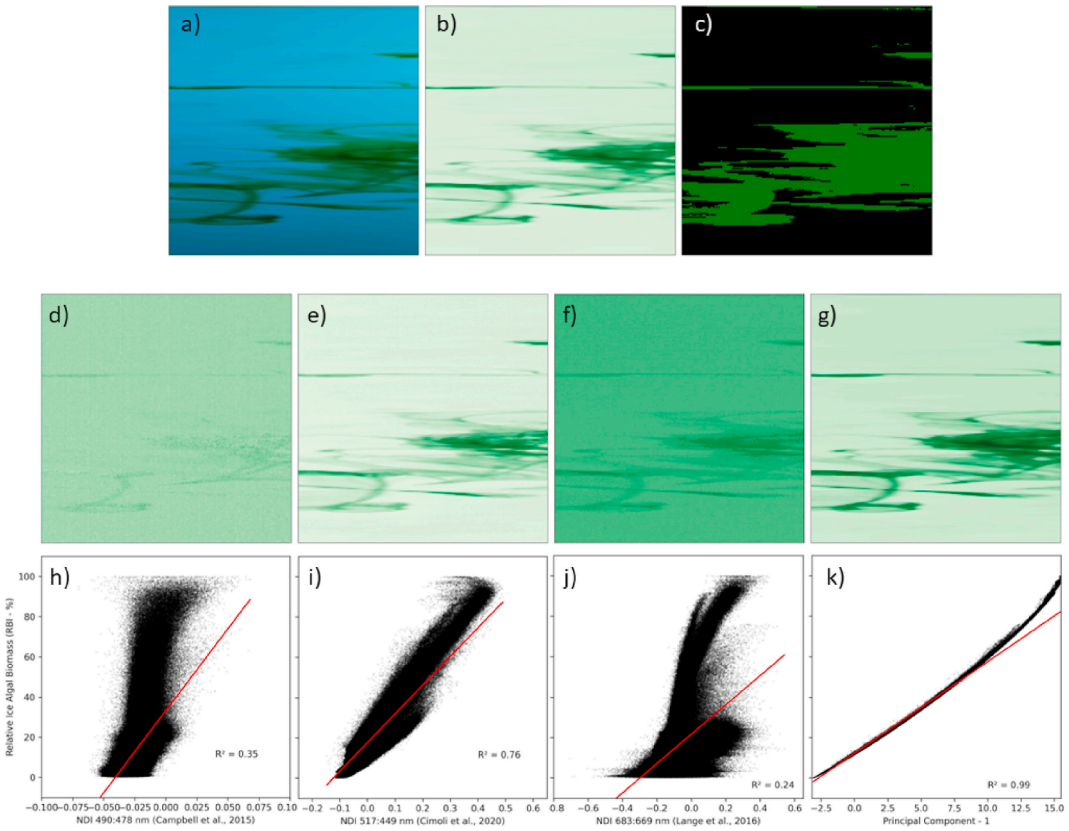

Fig. 12. Zoomed in images from corresponding region of the bottom inset (four white points) in Fig. 8 l (same inset also represented in Fig. 8 i, j, k) showing a) RGB composite; b) relative ice-algal biomass (RBI - %), c) SVM habitat classification; d) NDI 490:478 nm, Campbell et al. (2014), 2015); e) NDI 517:449 nm (Cimoli et al., 2020); f) NDI 683:669 nm (Lange et al., 2016); g) PC-1. NOTE: the same green colorscale was used and normalized to the minimum and maximum values. Scatterplots of Relative Ice algal biomass (RBI - %) vs.: h) NDI 490:478 nm (Campbell et al., 2014, 2015); i) NDI 517:449 nm (Cimoli et al., 2020); j) NDI 683:669 nm (Lange et al., 2016); k) PC-1. NOTE: r-squared shown in the bottom right of each scatterplot.

freshwater accumulation also have the potential to limit algal biomass due to impacts of salinity stress, where previous studies on species of ice algae have demonstrated a rapid drop in chl *a* following exposure of cells acclimated to typical ocean water salinities (e.g. 35) to salinities on the order of 10 (Campbell et al., 2019). The presence of a low salinity layer immediately beneath the ice would also limit algal growth by preventing the turbulent-driven supply of nutrients from depth that is important for bloom development (Duarte et al., 2022). Furthermore, the low porosity inherent to fresh ice of false bottoms (Smith et al., 2022) reduces habitable space and would further limit any colonization by ice algae.

We observed higher variability in relative ice algal biomass in level ice compared to the ridge flank (Fig. 6 e & f; Fig. 10). The lowest biomass for the level ice and the lowest biomass of both survey regions, were found along the keel of *Porridge*. Ridge keels experienced some of the most rapid melt rates during this period (e.g., Amundrud et al., 2006), which could explain the absence of algae in this region (Lavoie et al., 2005). This is also close to the false bottom layer, however, the beginning part of the level ice survey, which was also within an area of false bottoms, had average biomass levels. The other thing to note is that even if a freshwater layer is present, this does not exclude the possibility of algae since during the cruise we often observed a milky, brownish-green layer at the freshwater-seawater interface that was likely the result of stratification and accumulation of biological material, which would influence the spectral properties of the UHI observations and is something that may be difficult to distinguish from a sea ice algae signal. Thus, the presence of a freshwater layer could impact bottom ice algae as an environmental stressor or be a region where biological material accumulates each with important but different implications for the perceived UHI signal.

Despite having a high resolution and large coverage of surveyed regions it remains difficult to infer biophysical relationships. During this study and the final phase of the MOSAiC CO ice floe, we observed many physical changes of the sea ice and under-ice environment. First, we were in an advanced stage of melt. Second, we observed false bottoms and an under-ice freshwater layer during these UHI surveys (Salganik et al., 2023; Smith et al., 2022). These factors can impose salinity stress and changes in nutrient availability (Duarte et al., 2022). On top of this we have large spatial heterogeneity in ice thickness and light transmittance. All these factors influence physiology and ability of sea-ice algae to grow on the underside of sea ice. Yet, most of our understanding of sea-ice biogeochemical processes come from local point measurements and relating those point measurements to point measurements of snow depth, sea-ice thickness and light measurements.

3.6. Hypothetical sea ice coring along the UHI surveys

Here we provide a hypothetical case study of triplicate ice cores (ie., 50 × 50 pixel area ~ one ice core) extracted from five different locations (B1 to B5, Fig. 7 m Fig. 8 m) with an approximate center spacing of 10 m, along each RBI image. We then conducted an analysis of variance (ANOVA) to test for statistical differences between the sampled locations ($p < 0.05$). Our results indicated that the hypothetical ice core locations provided significantly different mean ($n = 3$) RBI results for both surveys depending on where you sampled your three ice cores (Fig. 13). These results emphasize the need for complementary spatial assessment of sea-ice algae biomass for ice core studies, particularly for temporal studies. These hypothetical ice coring locations could also represent sampling locations at different time points, similar to ice core time series during MOSAiC, which would complicate any interpretation of temporal variability since the spatial variability was likely significantly larger than any temporal changes. Therefore, our results provide important information on the spatial representativeness of ice core locations during the summer FYI times series locations of MOSAiC.

3.7. Limitations/caveats and future work

We note that the UHI surveys have not yet been spatially georectified to the ice floe coordinate system. To accurately georectify the UHI images, we need higher resolution multi-beam sonar bottom ice draft surveys aligned with ROV positioning and time synchronized with the UHI data. These processing steps are currently under development and will be applied in further analyses. This imposed limitations in the ability to provide quantitative spatial analyses. However, we could accurately align the across-track averages of RBI and integrated irradiance with ice draft as these represent spatially integrated signals and do not require higher resolution accuracy for positioning and georectification.

As mentioned earlier, the design of the MOSAiC central observatory limited our ability to take collocated ice cores within the ROV survey regions, which significantly limited our ability to develop a bio-optical algorithm for quantitative ice algal chl *a* biomass mapping. The SVM classification currently operates purely on a presence-absence basis, which limits its descriptive power. Enriching the model by introducing additional categories for algae, specifically low and high biomass classes, could enhance our understanding of algae's habitat preferences in connection to environmental properties. Nevertheless, the RBI results proved reliable as a proxy for ice algal biomass and a preliminary assessment of spatial variability for these two surveyed regions, and represent the foundation for further analyses.

Future work will involve processing the full one-month UHI time series (5 time points) in combination with ROV water parameter observations (e.g., salinity, temperature) and higher resolution multi-beam sonar ice draft surveys, which will include a more thorough examination of the spatio-temporal evolution of the under ice melt water layer, changes in ice draft (ie., melt rates) and false bottoms (Salganik et al., 2023; Smith et al., 2022). This will enable an unprecedented characterization of the spatio-temporal variability of sea-ice algae biomass in relation to key environmental parameters over a >100 m survey region at microscale spatial resolution (~1 cm).

4. Conclusions

In this study, we presented the first observations of Arctic sea ice using an underwater hyperspectral imager (UH) mounted on a ROV. Furthermore, we present a new unsupervised bio-optical quantification algorithm for hyperspectral surveys, the relative ice algal biomass index (RBI), using spectral mixture analysis (SMA) and the automated endmember extraction algorithm N-FINDR. We compare this method to a supervised machine learning habitat classification algorithm and literature-based proxies. The SVM habitat

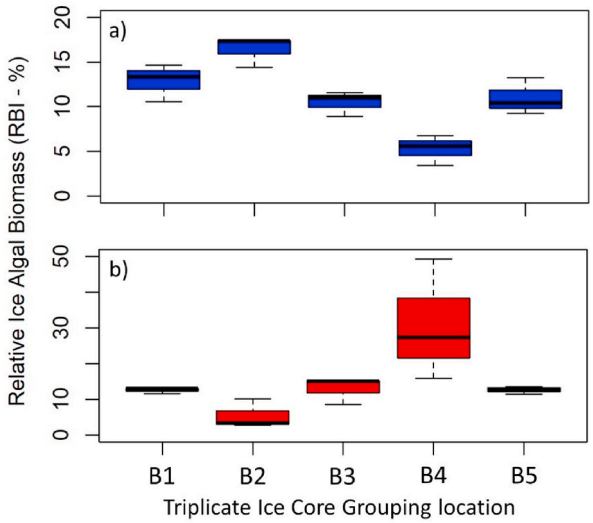

Fig. 13. Boxplots showing the hypothetical ice core relative ice algal biomass (RBI - %) for each ice core grouping location (Figs. 7 m and Fig. 8 m) along: a) ridge flank; and b) level ice surveys. NOTE: y-axes scales are different.

classification had some differences in the threshold between habitat classes, which was likely attributed to the training datasets. The RBI index showed excellent agreement to literature-based NDI ice-algal proxies and PCA results. Thus, demonstrating that the RBI is a reliable tool for ice algal biomass mapping even if calibration/validation ice core pigment data is not available.

Our biophysical characterization of the two surveyed regions showed an association of sea-ice algal biomass with sea-ice ridge features. Our surveys also indicate that ice algal spatial distribution may be influenced by ice melt rates, and the formation of under ice meltwater layers and false bottoms. With high spatial coverage (>100 m) at microscale resolution (~cm) we documented large spatial variability of summer Arctic sea-ice algae biomass and different patterns between adjacent but different coverage of ice habitats. We further demonstrate the need for improved understanding of sea-ice algal spatial variability as a complementary tool for sea-ice biogeochemical sampling using destructive ice core sampling.

5. Contributions

Contributed to conception and design: BAL, IM, CK, KC, MAG.

Contributed to acquisition of data: BAL, ES, IM, PA.

Contributed to analysis and interpretation of data: BAL, ES, IM, CK, MAG, KC, PA.

Drafted and/or revised the article: BAL drafted the first version of the manuscript, and all authors contributed to writing and revisions.

Approved the submitted version for publication: All authors.

Funding information

This work was supported by the Norwegian Polar Institute's Arctic Ocean program and the Research Council of Norway through projects CAATEX (grant no 280531) and HAVOC (grant no 280292). BAL was supported through the Fram Center Arctic Ocean flagship programme (project PHOTA 66014), funded by the Norwegian Ministry of Climate and Environment. CK and PA were funded by the German Federal Ministry of Education and Research (BMBF) project IceScan (03F0916A), while ROV operations were also funded by the Helmholtz strategic investment Frontiers in Arctic Marine Monitoring (FRAM).

Data accessibility statement

ROV multibeam sonar sea ice draft data (Katlein et al., 2022): DOI: https://doi.pangaea.de/10.1594/PANGAEA.945846 and Salganik et al. (2023). UHI data will be made available on PANGAEA at the following DOI. XXXXXXXXX before publications (status: currently in preparation). Python code for processing these data is available upon request.

Ethics statement

All authors declare that all ethical practices have been followed in relation to the development, writing, and publication of the article.

CRediT authorship contribution statement

Benjamin A. Lange: Conceptualization, Data curation, Formal analysis, Funding acquisition, Investigation, Methodology, Project administration, Resources, Software, Supervision, Validation, Visualization, Writing – original draft, Writing – review & editing. **Ilkka Matero:** Conceptualization, Data curation, Methodology, Software, Writing – review & editing. **Evgenii Salganik:** Data curation, Formal analysis, Investigation, Methodology, Writing – original draft, Writing – review & editing. **Karley Campbell:** Conceptualization, Funding acquisition, Investigation, Methodology, Validation, Writing – review & editing. **Christian Katlein:** Conceptualization, Data curation, Funding acquisition, Methodology, Software, Writing – review & editing. **Philipp Anhaus:** Methodology, Software, Validation, Writing – review & editing, Data curation, Investigation. **Janina Osanen:** Conceptualization, Formal analysis, Methodology, Software, Writing – review & editing. **Mats A. Granskog:** Conceptualization, Data curation, Formal analysis, Funding acquisition, Investigation, Project administration, Supervision, Writing – review & editing.

Declaration of competing interest

The authors declare that they have no known competing financial interests or personal relationships that could have appeared to influence the work reported in this paper.

Data availability

Data are currently in the process of being uploaded to a open access data reposity with DOI to be included in the published version of the manuscript.

Acknowledgements

This work was carried out and data used in this manuscript was produced as part of the international Multidisciplinary drifting Observatory for the Study of the Arctic Climate (MOSAiC) with the tag MOSAiC 20192020. We thank all persons involved in the expe-

dition of the Research Vessel Polarstern during MOSAiC in 2019–2020 (AWI_PS122_00) as listed in (Nixdorf et al., 2021). Special thanks to Felix Linhardt for help with ROV-UHI integration and Julia Regnery for support with ROV operations.

References

Amundrud, T.L., Melling, H., Ingram, R.G., Allen, S.E., 2006. The effect of structural porosity on the ablation of sea ice ridges. J. Geophys. Res. 111. https://doi.org/10.1029/2005jc002895.

Arrigo, K.R., van Dijken, G.L., 2015. Continued increases in Arctic Ocean primary production. Prog. Oceanogr. 136, 60–70. https://doi.org/10.1016/j.pocean.2015.05.002.

Campbell, K., Lange, B.A., Landy, J.C., Katlein, C., Nicolaus, M., Anhaus, P., Matero, I., Gradinger, R., Charette, J., Duerksen, S., Tremblay, P., Rysgaard, S., Tranter, M., Haas, C., Michel, C., 2022. Net heterotrophy in High Arctic first-year and multi-year spring sea ice. Elementa: Sci. Anthropol. 10. https://doi.org/10.1525/elementa.2021.00040.

Campbell, K., Mundy, C.J., Barber, D.G., Gosselin, M., 2014. Remote estimates of ice algae biomass and their response to environmental conditions during spring melt. Arctic 67, 375. https://doi.org/10.14430/arctic4409.

Campbell, K., Mundy, C.J., Barber, D.G., Gosselin, M., 2015. Characterizing the sea ice algae chlorophyll a–snow depth relationship over Arctic spring melt using transmitted irradiance. J. Mar. Syst. 147, 76–84. https://doi.org/10.1016/j.jmarsys.2014.01.008.

Campbell, K., Mundy, C.J., Juhl, A.R., Dalman, L.A., Michel, C., Galley, R.J., Else, B.E., Geilfus, N.X., Rysgaard, S., 2019. Melt procedure affects the photosynthetic response of Sea Ice algae. Front. Earth Sci. 7. https://doi.org/10.3389/feart.2019.00021.

Chennu, A., Farber, P., De'ath, G., de Beer, D., Fabricius, K.E., 2017. A diver-operated hyperspectral imaging and topographic surveying system for automated mapping of benthic habitats. Sci. Rep. 7, 7122. https://doi.org/10.1038/s41598-017-07337-y.

Cimoli, E., Lucieer, A., Meiners, K.M., Lund-Hansen, L.C., Kennedy, F., Martin, A., McMinn, A., Lucieer, V., 2017. Towards improved estimates of sea-ice algal biomass: experimental assessment of hyperspectral imaging cameras for under-ice studies. Ann. Glaciol. 58, 68–77. https://doi.org/10.1017/aog.2017.6.

Cimoli, E., Lucieer, V., Meiners, K.M., Chennu, A., Castrisios, K., Ryan, K.G., Lund-Hansen, L.C., Martin, A., Kennedy, F., Lucieer, A., 2020. Mapping the in situ microspatial distribution of ice algal biomass through hyperspectral imaging of sea-ice cores. Sci. Rep. 10, 21848. https://doi.org/10.1038/s41598-020-79084-6.

Cimoli, E., Meiners, K.M., Lucieer, A., Lucieer, V., 2019. An under-ice hyperspectral and RGB imaging system to capture fine-scale biophysical properties of Sea Ice. Rem. Sens. 11. https://doi.org/10.3390/rs11232860.

Craig, S.E., Jones, C.T., Li, W.K.W., Lazin, G., Horne, E., Caverhill, C., Cullen, J.J., 2012. Deriving optical metrics of coastal phytoplankton biomass from ocean colour. Rem. Sens. Environ. 119, 72–83. https://doi.org/10.1016/j.rse.2011.12.007.

Duarte, P., Assmy, P., Campbell, K., Sundfjord, A., 2022. The importance of turbulent ocean–sea ice nutrient exchanges for simulation of ice algal biomass and production with CICE6.1 and Icepack 1.2. Geosci. Model Dev. (GMD) 15, 841–857. https://doi.org/10.5194/gmd-15-841-2022.

Dumke, I., Nornes, S.M., Purser, A., Marcon, Y., Ludvigsen, M., Ellefmo, S.L., Johnsen, G., Søreide, F., 2018a. First hyperspectral imaging survey of the deep seafloor: high-resolution mapping of manganese nodules. Rem. Sens. Environ. 209, 19–30. https://doi.org/10.1016/j.rse.2018.02.024.

Dumke, I., Purser, A., Marcon, Y., Nornes, S.M., Johnsen, G., Ludvigsen, M., Soreide, F., 2018b. Underwater hyperspectral imaging as an in situ taxonomic tool for deep-sea megafauna. Sci. Rep. 8, 12860. https://doi.org/10.1038/s41598-018-31261-4.

Fernández-Méndez, M., Katlein, C., Rabe, B., Nicolaus, M., Peeken, I., Bakker, K., Flores, H., Boetius, A., 2015. Photosynthetic production in the Central Arctic during the record sea-ice minimum in 2012. Biogeosciences 12, 2897–2945. https://doi.org/10.5194/bgd-12-2897-2015.

Fernández-Méndez, M., Olsen, L.M., Kauko, H.M., Meyer, A., Rösel, A., Merkouriadi, I., Mundy, C.J., Ehn, J.K., Johansson, A.M., Wagner, P.M., Ervik, Å., Sorrell, B.K., Duarte, P., Wold, A., Hop, H., Assmy, P., 2018. Algal hot spots in a changing Arctic Ocean: sea-Ice ridges and the snow-ice interface. Front. Mar. Sci. 5. https://doi.org/10.3389/fmars.2018.00075.

Freitas, S., Silva, H., Silva, E., 2021. Remote hyperspectral imaging acquisition and characterization for marine litter detection. Rem. Sens. 13. https://doi.org/10.3390/rs13132536.

Gerland, S., Barber, S., Meier, W., Mundy, C.J., Holland, M., Kern, S., Li, Z., Michel, C., Perovich, D., Tamura, T., 2019. Essential gaps in the understanding of the roles and functions of Arctic sea ice. Environ. Res. Lett. https://doi.org/10.1088/1748-9326/ab09b3.

Gosselin, M., Levasseur, M., Wheeler, P.A., Horner, R.A., Booth, B.C., 1997. New measurements of phytoplankton and ice algal production in the Arctic Ocean. Deep Sea Res. Part II Top. Stud. Oceanogr. 44, 1623–1644. https://doi.org/10.1016/S0967-0645(97)00054-4.

Itkin, P., Spreen, G., Cheng, B., Doble, M., Girard-Ardhuin, F., Haapala, J., Hughes, N., Kaleschke, L., Nicolaus, M., Wilkinson, J., 2017. Thin ice and storms: sea ice deformation from buoy arrays deployed during N-ICE2015. J. Geophys. Res.: Oceans 122, 4661–4674. https://doi.org/10.1002/2016jc012403.

Järvinen, O., Leppäranta, M., 2011. Transmission of solar radiation through the snow cover on floating ice. J. Glaciol. 57, 861–870. https://doi.org/10.3189/002214311798043843.

Ji, L., Geng, X., Sun, K., Zhao, Y., Gong, P., 2015. Modified N-FINDR endmember extraction algorithm for remote-sensing imagery. Int. J. Rem. Sens. 36, 2148–2162. https://doi.org/10.1080/01431161.2015.1034895.

Johnsen, G., Volent, Z., Dierssen, H., Pettersen, R., Ardelan, M.V., Søreide, F., Fearns, P., Ludvigsen, M., Moline, M., 2013. 20 - underwater hyperspectral imagery to create biogeochemical maps of seafloor properties. In: Watson, J., Zielinski, O. (Eds.), Subsea Optics and Imaging. Woodhead Publishing, p. 508–540e. https://doi.org/10.1533/9780857093523.3.508.

Katlein, C., Anhaus, P., Arndt, S., Krampe, D., Lange, B.A., Matero, I., Regnery, J., Rohde, J., Schiller, M., Nicolaus, M., 2022. Sea-ice draft during the MOSAiC expedition 2019/20. In: PANGAEA. https://doi.org/10.1594/PANGAEA.945846.

Katlein, C., Arndt, S., Belter, H.J., Castellani, G., Nicolaus, M., 2019. Seasonal evolution of light transmission distributions through arctic Sea Ice. J. Geophys. Res.: Oceans 124, 5418–5435. https://doi.org/10.1029/2018jc014833.

Katlein, C., Fernández-Méndez, M., Wenzhöfer, F., Nicolaus, M., 2014. Distribution of algal aggregates under summer sea ice in the Central Arctic. In: Polar Biology. pp. 719–731. https://doi.org/10.1007/s00300-014-1634-3.

Katlein, C., Schiller, M., Belter, H.J., Coppolaro, V., Wenslandt, D., Nicolaus, M., 2017. A new remotely operated sensor platform for interdisciplinary observations under Sea Ice. Front. Mar. Sci. 4. https://doi.org/10.3389/fmars.2017.00281.

Kohlbach, D., Graeve, M., Lange, B.A., David, C., Peeken, I., Flores, H., 2016. The importance of ice algae-produced carbon in the central Arctic Ocean ecosystem: food web relationships revealed by lipid and stable isotope analyses. Limnol. Oceanogr. 2027–2044. https://doi.org/10.1002/lno.10351.

Kwok, R., 2018. Arctic sea ice thickness, volume, and multiyear ice coverage: losses and coupled variability (1958–2018). Environ. Res. Lett. 13. https://doi.org/10.1088/1748-9326/aae3ec.

Lange, B.A., Flores, H., Michel, C., Beckers, J.F., Bublitz, A., Casey, J.A., Castellani, G., Hatam, I., Reppchen, A., Rudolph, S.A., Haas, C., 2017a. Pan-Arctic sea ice-algal chl a biomass and suitable habitat are largely underestimated for multi-year ice. Global Change Biol. https://doi.org/10.1111/gcb.13742.

Lange, B.A., Haas, C., Charette, J., Katlein, C., Campbell, K., Duerksen, S., Coupel, P., Anhaus, P., Jutila, A., Tremblay, P.O.G., Carlyle, C.G., Michel, C., 2019. Contrasting ice algae and snow-dependent irradiance relationships between first-year and multi-year sea ice. Geophys. Res. Lett. https://doi.org/10.1029/2019GL082873.

Lange, B.A., Katlein, C., Castellani, G., Fernández-Méndez, M., Nicolaus, M., Peeken, I., Flores, H., 2017b. Characterizing spatial variability of ice algal chlorophyll a and net primary production between Sea Ice habitats using horizontal profiling platforms. Front. Mar. Sci.: Ocean Obs. https://doi.org/10.3389/fmars.2017.00349.

Lange, B.A., Katlein, C., Nicolaus, M., Peeken, I., Flores, H., 2016. Sea ice algae chlorophyll a concentrations derived from under-ice spectral radiation profiling platforms. In: Journal of Geophysical Research: Oceans. pp. 8511–8534. https://doi.org/10.1002/2016JC011991.

Lange, B.A., Salganik, E., Macfarlane, A.R., Schneebeli, M., Høyland, K., Gardner, J., Müller, O., Divine, D.V., Kohlbach, D., Katlein, C., Granskog, M.A., 2023. Snowmelt contributes to Arctic first-year ice ridge mass balance and rapid consolidation during summer melt. In: Elementa: Science of the Anthropocene. https://doi.org/10.1525/elementa.2022.00037.

Lannuzel, D., Tedesco, L., van Leeuwe, M., Campbell, K., Flores, H., Delille, B., Miller, L., Stefels, J., Assmy, P., Bowman, J., Brown, K., Castellani, G., Chierici, M.,

Crabeck, O., Damm, E., Else, B., Fransson, A., Fripiat, F., Geilfus, N.-X., Jacques, C., Jones, E., Kaartokallio, H., Kotovitch, M., Meiners, K., Moreau, S., Nomura, D., Peeken, I., Rintala, J.-M., Steiner, N., Tison, J.-L., Vancoppenolle, M., Van der Linden, F., Vichi, M., Wongpan, P., 2020. The future of Arctic sea-ice biogeochemistry and ice-associated ecosystems. Nat. Clim. Change 10, 983–992. https://doi.org/10.1038/s41558-020-00940-4.

Lavoie, D., Denman, K., Michel, C., 2005. Modeling ice algal growth and decline in a seasonally ice-covered region of the Arctic (Resolute Passage, Canadian Archipelago). In: Journal of Geophysical Research. C11009. https://doi.org/10.1029/2005JC002922.

Legendre, L., Gosselin, M., 1991. In situ spectroradiometric estimation of microalgal biomass in first-year sea ice. Polar Biol. 11, 113–115. https://doi.org/10.1007/BF00234273.

Lund-Hansen, L.C., Hawes, I., Nielsen, M.H., Sorrell, B.K., 2016. Is colonization of sea ice by diatoms facilitated by increased surface roughness in growing ice crystals? Polar Biol. 40, 593–602. https://doi.org/10.1007/s00300-016-1981-3.

Matrai, P., Apollonio, S., 2013. New estimates of microalgae production based upon nitrate reductions under sea ice in Canadian shelf seas and the Canada Basin of the Arctic Ocean. In: Marine Biology. pp. 1297–1309. https://doi.org/10.1007/s00227-013-2181-0.

Meiners, K.M., Arndt, S., Bestley, S., Krumpen, T., Ricker, R., Milnes, M., Newbery, K., Freier, U., Jarman, S., King, R., Proud, R., Kawaguchi, S., Meyer, B., 2017. Antarctic pack ice algal distribution: floe-scale spatial variability and predictability from physical parameters. Geophys. Res. Lett. 44, 7382–7390. https://doi.org/10.1002/2017GL074346.

Melbourne-Thomas, J., Meiners, K.M., Mundy, C.J., Schallenberg, C., Tattersall, K.L., Dieckmann, G.S., 2016. Corrigendum: Algorithms to Estimate Antarctic Sea Ice Algal Biomass from Under-ice Irradiance Spectra at Regional Scales. p. 261. https://doi.org/10.3354/meps11396.

Miller, L.A., Fripiat, F., Else, B.G.T., Bowman, J.S., Brown, K.A., Collins, R.E., Ewert, M., Fransson, A., Gosselin, M., Lannuzel, D., Meiners, K.M., Michel, C., Nishioka, J., Nomura, D., Papadimitriou, S., Russell, L.M., Sørensen, L.L., Thomas, D.N., Tison, J.-L., van Leeuwe, M.A., Vancoppenolle, M., Wolff, E.W., Zhou, J., 2015. Methods for biogeochemical studies of sea ice: the state of the art, caveats, and recommendations. Elementa: Sci. Anthropol. 3, 000038. https://doi.org/10.12952/journal.elementa.000038.

Mogstad, A.A., Johnsen, G., Ludvigsen, M., 2019. Shallow-water habitat mapping using underwater hyperspectral imaging from an unmanned surface vehicle: a pilot study. Rem. Sens. 11. https://doi.org/10.3390/rs11060685.

Mogstad, A.A., Ødegård, Ø., Nornes, S.M., Ludvigsen, M., Johnsen, G., Sørensen, A.J., Berge, J., 2020. Mapping the historical shipwreck figaro in the high arctic using underwater sensor-carrying robots. Rem. Sens. 12. https://doi.org/10.3390/rs12060997.

Montes-Herrera, J.C., Cimoli, E., Cummings, V., Hill, N., Lucieer, A., Lucieer, V., 2021. Underwater hyperspectral imaging (UHI): a review of systems and applications for proximal seafloor ecosystem studies. Rem. Sens. 13. https://doi.org/10.3390/rs13173451.

Mundy, C.J., Ehn, J.K., Barber, D.G., Michel, C., 2007. Influence of snow cover and algae on the spectral dependence of transmitted irradiance through Arctic landfast first-year sea ice. J. Geophys. Res. 112, C03007. https://doi.org/10.1029/2006JC003683.

Nicolaus, M., Perovich, D.K., Spreen, G., Granskog, M.A., von Albedyll, L., Angelopoulos, M., Anhaus, P., Arndt, S., Belter, H.J., Bessonov, V., Birnbaum, G., Brauchle, J., Calmer, R., Cardellach, E., Cheng, B., Clemens-Sewall, D., Dadic, R., Damm, E., de Boer, G., Demir, O., Dethloff, K., Divine, D.V., Fong, A.A., Fons, S., Frey, M.M., Fuchs, N., Gabarró, C., Gerland, S., Goessling, H.F., Gradinger, R., Haapala, J., Haas, C., Hamilton, J., Hannula, H.-R., Hendricks, S., Herber, A., Heuzé, C., Hoppmann, M., Høyland, K.V., Huntemann, M., Hutchings, J.K., Hwang, B., Itkin, P., Jacobi, H.-W., Jaggi, M., Jutila, A., Kaleschke, L., Katlein, C., Kolabutin, N., Krampe, D., Kristensen, S.S., Krumpen, T., Kurtz, N., Lampert, A., Lange, B.A., Lei, R., Light, B., Linhardt, F., Liston, G.E., Loose, B., Macfarlane, A.R., Mahmud, M., Matero, I.O., Maus, S., Morgenstern, A., Naderpour, R., Nandan, V., Niubom, A., Oggier, M., Oppelt, N., Pätzold, F., Perron, C., Petrovsky, T., Pirazzini, R., Polashenski, C., Rabe, B., Raphael, I.A., Regnery, J., Rex, M., Ricker, R., Riemann-Campe, K., Rinke, A., Rohde, J., Salganik, E., Scharien, R.K., Schiller, M., Schneebeli, M., Semmling, M., Shimanchuk, E., Shupe, M.D., Smith, M.M., Smolyanitsky, V., Sokolov, V., Stanton, T., Stroeve, J., Thielke, L., Timofeeva, A., Tonboe, R.T., Tavri, A., Tsamados, M., Wagner, D.N., Watkins, D., Webster, M., Wendisch, M., 2022. Overview of the MOSAiC expedition. Elementa: Sci. Anthropol. 10. https://doi.org/10.1525/elementa.2021.000046.

Nixdorf, U., Dethloff, K., Rex, M., Shupe, M., Sommerfeld, A., Perovich, D.K., Nicolaus, M., Heuzé, C., Rabe, B., Loose, B., Damm, E., Gradinger, R., Fong, A., Maslowski, W., Rinke, A., Kwok, R., Spreen, G., Wendisch, M., Herber, A., Boetius, A., 2021. MOSAiC Extended Acknowledgement. Zenodo. https://doi.org/10.5281/zenodo.5541624.

Perovich, D.K., 1996. The optical properties of Sea Ice, rep. 96-1. In: Cold Regions Research and Engineering Laboratory.

Salganik, E., Katlein, C., Lange, B.A., Matero, I., Lei, R., Fong, A.A., Fons, S.W., Divine, D., Oggier, M., Castellani, G., Bozzato, D., Chamberlain, E.J., Hoppe, C.J.M., Müller, O., Gardner, J., Rinke, A., Pereira, P.S., Ulfsbo, A., Marsay, C., Webster, M.A., Maus, S., Høyland, K.V., Granskog, M.A., 2023. Temporal evolution of under-ice meltwater layers and false bottoms and their impact on summer Arctic sea ice mass balance. Elementa: Sci. Anthropol. 11. https://doi.org/10.1525/elementa.2022.00035.

Smith, M.M., von Albedyll, L., Raphael, I.A., Lange, B.A., Matero, I., Salganik, E., Webster, M.A., Granskog, M.A., Fong, A., Lei, R.B., Light, B., 2022. Quantifying false bottoms and under-ice meltwater layers beneath Arctic summer sea ice with fine-scale observations. Elementa Sci. Anthropol. 10. https://doi.org/10.1525/elementa.2021.000116.

Søreide, J.E., Leu, E.V.A., Berge, J., Graeve, M., Falk-Petersen, S., 2010. Timing of blooms, algal food quality and Calanus glacialis reproduction and growth in a changing Arctic. Global Change Biol. 3154–3163. https://doi.org/10.1111/j.1365-2486.2010.02175.x.

Stroeve, J., Notz, D., 2018. Changing state of Arctic sea ice across all seasons. Environ. Res. Lett. 13. https://doi.org/10.1088/1748-9326/aade56.

Summers, N., Johnsen, G., Mogstad, A., Løvås, H., Fragoso, G., Berge, J., 2022. Underwater hyperspectral imaging of arctic macroalgal habitats during the polar night using a novel mini-ROV-UHI portable system. Rem. Sens. 14. https://doi.org/10.3390/rs14061325.

Tait, L., Bind, J., Charan-Dixon, H., Hawes, I., Pirker, J., Schiel, D., 2019. Unmanned aerial vehicles (UAVs) for monitoring macroalgal biodiversity: comparison of RGB and multispectral imaging sensors for biodiversity assessments. Rem. Sens. 11. https://doi.org/10.3390/rs11192332.

Taylor, B.B., Taylor, M.H., Dinter, T., Bracher, A., 2013. Estimation of relative phycoerythrin concentrations from hyperspectral underwater radiance measurements—A statistical approach. J. Geophys. Res.: Oceans 118, 2948–2960. https://doi.org/10.1002/jgrc.20201.

Thomas, C.W., 1963. On the transfer of visible radiation through sea ice and snow. J. Glaciol. 4, 481–484.

Wadhams, P., Toberg, N., 2012. Changing characteristics of arctic pressure ridges. Polar Sci. 71–77. https://doi.org/10.1016/j.polar.2012.03.002.

Wang, S.W., Budge, S.M., Iken, K., Gradinger, R.R., Springer, A.M., Wooller, M.J., 2015. Importance of sympagic production to Bering Sea zooplankton as revealed from fatty acid-carbon stable isotope analyses. Mar. Ecol. Prog. Ser. 518, 31–50. https://doi.org/10.3354/meps11076.

Wongpan, P., Meiners, K.M., Langhorne, P.J., Heil, P., Smith, I.J., Leonard, G.H., Massom, R.A., Clementson, L.A., Haskell, T.G., 2018. Estimation of antarctic land-fast Sea Ice algal biomass and snow thickness from under-ice radiance spectra in two contrasting areas. J. Geophys. Res.: Oceans 123, 1907–1923. https://doi.org/10.1002/2017jc013711.